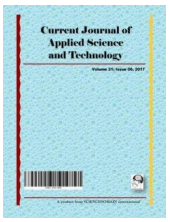

Current Journal of Applied Science and Technology

24(5): 1-17, 2017; Article no.CJAST.37474
Previously known as British Journal of Applied Science & Technology
ISSN: 2231-0843, NLM ID: 101664541

Rectangular Hollow Section (RHS) Rings under Lateral Compressive Loading between Platens and Wearpads

Neha Arieckal Jacob[1*] and Sangarappillai Sivaloganathan[1]

[1]College of Engineering, United Arab Emirates University, P.O.Box 15551, Al Ain, United Arab Emirates.

Authors' contributions

This work is part of author NAJ PhD research, and was carried out in collaboration with author SS. The strategy, design and analysis were discussed by both authors and the analysis was executed by author NAJ. Both authors read and approved the final manuscript.

Article Information

DOI: 10.9734/CJAST/2017/37474
Editor(s):
(1) Rodolfo Dufo Lopez, Professor, Electrical Engineering Department, University of Zaragoza, Spain.
Reviewers:
(1) Avijit Sinha, Dalhousie University, Canada.
(2) J. Dario Aristizabal-Ochoa, National University of Colombia, Colombia.
Complete Peer review History: http://www.sciencedomain.org/review-history/22013

Original Research Article

Received 18th October 2017
Accepted 3rd November 2017
Published 22nd November 2017

ABSTRACT

Aims: To investigate the buckling behavior of RHS Rings, under two kinds of transverse loading (a) between platens and (b) between wearpads, by experimentation and through Finite Element Analysis(FEA).
Place and Duration of Study: College of Engineering, UAE University, between December 2015 to June 2017.
Methodology: Experimental studies on sample RHS Rings compressed transversely between platens and wearpads were conducted. From the experimental observations, the behavior of RHS rings under both these types of loadings was hypothesized and explained theoretically. FE models were built to represent the experimental tests.
Results: Experimental and FEA results showed load-displacement curves with three distinct regions, namely the elastic region, elasto-plastic region and the post-yield region under both kinds of loading. However, the maximum load under wearpad loading was much lower when a similar RHS Ring is considered under platen loading. The behavior of RHS Rings is explained theoretically by considering the RHS Rings as an assemblage of horizontal beams and vertical columns.
Conclusion: Transverse compression of RHS Rings between platens cause each member columns

**Corresponding author: E-mail: nehajacob@uaeu.ac.ae;*

and beams of the ring to be subjected to end moments and end reaction forces. Additional end moments are induced when RHS Rings are compressed between wearpads causing a reduction in the RHS Ring load carrying capacity.

Keywords: Buckling behavior; RHS rings; transverse loading; platens; wearpads; experimentation; finite element analysis; load-displacement curves.

1. INTRODUCTION

A RHS ring is a small part of a RHS piece with relatively small length when compared to the cross-sectional width and height. The structural connectivity of the ring however is similar to that of a RHS piece.

A ring can be considered as an assemblage of columns and beams while a RHS piece can be considered as an assemblage of vertical and horizontal plates as shown in Fig. 1.

Rings have their applications in a stand-alone fashion and as part of other structural members. In a telescopic beam for example it can form part of the overlap region, which transmits the load from the outer beam to the inner beam through the wear-pads as shown in Fig. 2.

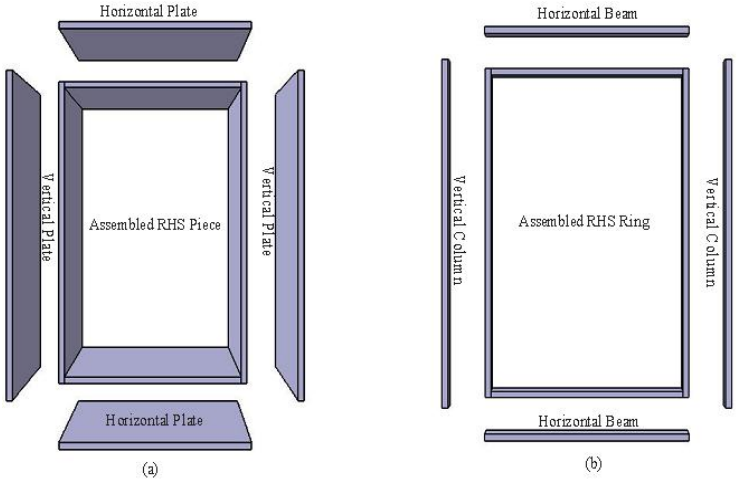

Fig. 1. (a) RHS piece and (b) RHS ring as assemblages of simple structural members

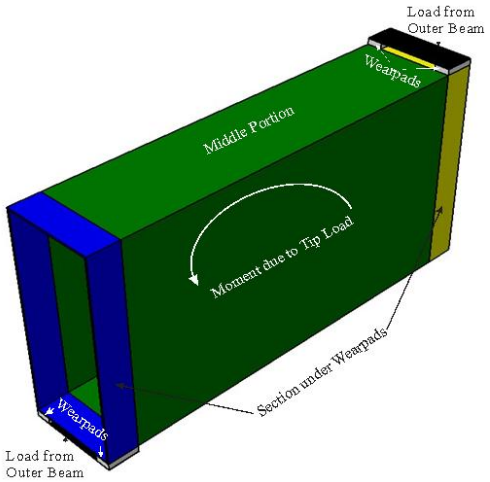

Fig. 2. Division of the overlap section

In such applications, the load is compressive in nature and as such the ring may collapse before the stresses in it reach the yielding values. This makes the investigation of rings under compressive loads between platens and between wearpads necessary. This paper aims to explain the behavior of RHS Rings under transverse compressive loads and to establish an FE method to investigate this behavior. Further, a theoretical explanation of the behavior of RHS rings under transverse loads is proposed. Methods used to achieve these objectives include physical experimentation, Finite Element Analysis and theoretical considerations.

2. LITERATURE SURVEY

Lateral compression of round, square and rectangular tubes allow for efficient energy absorption, and have hence been the subject of extensive research with respect to their plastic collapse and energy absorption capacity.

The phenomena associated with the crushing of metal tubes between rigid plates was studied by Reid and Reddy in [1]. Sinha and Chitkara [2] obtained the plastic collapse load for square rings from the stability analysis of the vertical arms of the tubes. In it the post-collapse load deformation was derived by assuming plastic hinges at mid points of each of the arms. Gupta and Khullar [3] presented an improved analysis for obtaining the collapse load of square and rectangular tubes, by considering the initial out of straightness of the arms and the comer roundness of the sections. In [4], Gupta and Khullar also studied the mechanisms of plastic collapse of orthogonal and non-orthogonal cross-layered systems of square and rectangular aluminum tubes by subjecting them to lateral compression. Gupta and Ray [5] studied the large deformation behavior and collapse load of empty and filled aluminum tubes of square cross section subjected to lateral loading between two rigid plates. They considered plastic hinges formation for obtaining peak load and frictional force between platen and tube and equated slopes of webs and flanges for theoretical analysis. The deformation, load-compression response and the energy absorbed during collapse of square tubes compressed between an indenter and a rigid platen are discussed by Gupta and Sinha in [6]. In [7], when compressed under different indenters, and placed on a rigid flat surface, Gupta and Sinha studied square tubes of aluminum and mild steel, for deformation, load-compression response and the energy absorbed during collapse. Gupta and Khullar presented a study on the collapse behavior of square or rectangular tubes subjected to transverse loading by narrow width indenters, placed in orthogonal and non-orthogonal positions in [8,9]. Experimental and computational investigation of the deformation and energy absorbing behavior of rectangular and square tubes of aluminum and mild steel under lateral compression was studied in [10] by Gupta et al.

More recently, the crushing mechanism and plastic analysis of thin-walled equilateral triangular tubes being laterally compressed was studied in [11] by Fan, Hong et al. Daw-Kwei Leu [12] studied the buckling mechanism of aluminum and clad tubes subjected to lateral compression along with the effect of various parameters on the process using FEA. The lateral crushing behavior and theoretical prediction of thin-walled rectangular and square tubes is given in [13].

While this group of papers concentrate on the analysis of tubes the plastic area, the behavior of the RHS tubes is not detailed before the maximum load. Therefore, this paper concentrates on the behavior of the RHS Rings before the maximum load capacity is reached. The recommended theoretical analysis in this paper is adapted from the ‘collapse load of empty tubes’ given by Gupta and Ray in [6].

3. EXPERIMENTATION

This section describes the experimental work carried out on RHS rings between platens and wearpads. A ring is made up of strips whose width and thickness are small compared to their lengths.

RHS Rings with cross sectional dimensions 350mm x 150mm with a length of 10mm, corner radius of 5mm and a uniform thickness of 3mm were subjected to compressive loads in these experiments. CRCA (Cold Rolled Cold Annealed) MS strips with 3mm thickness and 10mm width were bent on a press brake to form the RHS Ring sections. A single center weld on the top flange of each section closed the ring section. The thickness measurement taken using a Vernier calipers at points A-J shown in Fig. 3 are listed for RHS Rings compressed between platens in Table 1 and in Table 3 for RHS Rings compressed between wearpads.

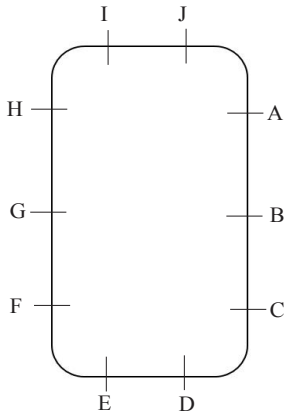

Fig. 3. Thickness measurement points

An MTS machine (model: 20/H) was used for the experiments. The downward head movement was maintained at a velocity of 0.5 mm/min to apply the load in all the trials. The MTS machine had a capacity of 1000 kN and is equipped with various load heads (Head capacity: 5 kN, 100 kN, 1000 kN) for different load capacities. The load head was changed to a 5 kN capacity for more accurate readings as the maximum load capacity of the Rings was expected to be 1.04 kN (from the initial FEA data). On completion of each experiment, the output was obtained as load-displacement graphs in excel format. The bottom platen of the machine had a 150 mm diameter while the load was applied at the top through a 50 mm diameter.

3.1 Experiment 1 – Compression of RHS Rings between Platens

3.1.1 Thickness measurement

The thickness measurement taken using a Vernier calipers at points A-J shown in Fig. 3 are listed for three RHS Ring specimens compressed between platens in Table 1.

3.1.2 Description of the process

The assembly of the RHS Ring compressed between platens is as shown in Fig. 4(d). The assembly consists of a RHS Ring placed between the top and bottom platens. The top platen has a shallow groove on its upper surface to accommodate the load distributor. The load distributor has a spherical upper surface (in contact with the machine load-applying cylinder) and a flat lower surface (in contact with the platen on top of the RHS Ring). This arrangement allows for a better, more uniform distribution of load on the RHS Ring.

The assembly was placed on the MTS machine lower platen while the load was applied by the machine top cylinder. The load was continuously applied till the maximum load value was reached after which the load was released and the load-displacement plot obtained as an output.

3.1.3 Physical behavior

Platens are flat surfaces that apply a uniformly distributed load on the flat, top and bottom flanges of the RHS Ring placed between them. But if the top flange starts sagging and the bottom flange starts hogging, the load distribution will concentrate on the peripheral areas which are still in contact with the platens. In short, the platens will transmit forces through the areas that maintain contact with them. This is elaborated further in Fig. 4 and in the explanation given below.

The flanges and the webs at the beginning had no deflection and were at right angles to each other as shown in Fig. 4 (a). The platens were in full surface contact with the RHS flanges at this stage. Fig. 4 (b) shows that as the load is increased, the top flange begins to sag (like a beam under transverse loading) and the bottom flange begins to hog causing the flanges to lose contact with the platens in the middle. The webs also begin to bulge outwards. Further increase in the loading is marked by an obvious and exaggerated deformation on all four strips of the RHS Ring – the two flanges and the two webs. The shape of the RHS Ring is shown in Fig. 4 (c). In the last stage, after the maximum load is passed, the RHS Ring consists of webs hinged at mid-height and bent flanges as shown in Fig. 4 (d).

Table 1. Thickness measurements of RHS Rings between platens

Specimen	Thickness (mm)									
	A	B	C	D	E	F	G	H	I	J
SR1	2.97	2.97	3.01	2.94	2.99	2.97	3.03	3.09	3.05	3.02
SR2	2.94	2.96	2.90	2.83	2.89	2.89	2.88	2.85	2.82	2.88
SR3	2.83	2.77	2.86	2.81	2.83	2.75	2.81	2.82	2.74	2.79

When the web of the RHS Ring is bent, consider the right web. The bent shape is like the one showed in Fig. 5 (a). If this is cut by an imaginary plane at the middle, the free body diagram of the upper half will be as shown in Fig. 5 (b).

The entire cross section will experience the same compressive stress P/A. In addition, the outermost fiber on the outer side will have maximum tensile stress while the outermost fiber on the inner side will have the compressive stress caused due to the bending moment 'Py'. This will result in a bigger compressive stress at the outermost fiber on the inner side. Yielding therefore can be expected to begin at the inner sides of the flanges at the mid-height where 'y' is maximum.

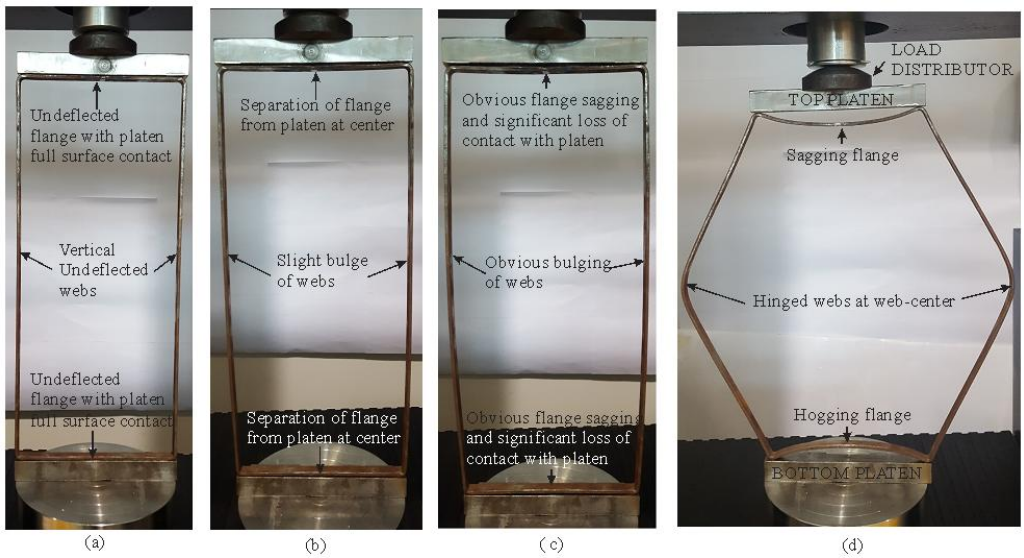

Fig. 4. RHS Ring between platens at (a) Stage 1 (b) Stage 2 (c) Stage 3 (d) Stage 4

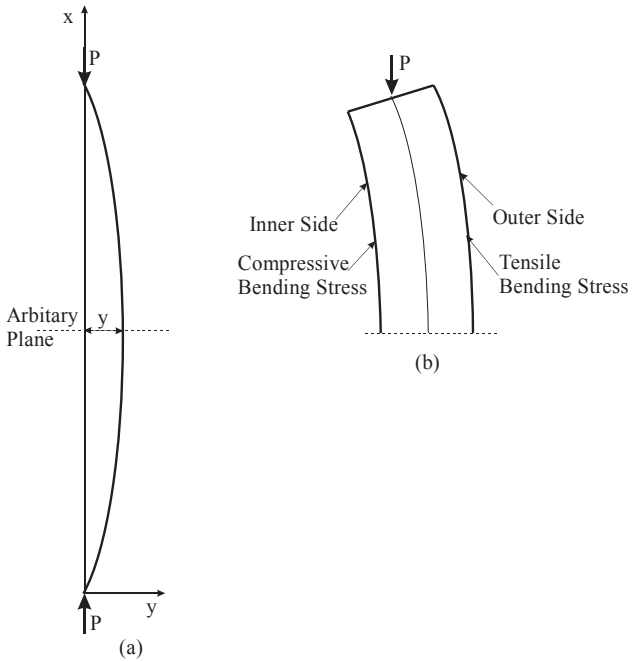

Fig. 5. (a) Bent shape and (b) Difference in stresses in Right web

3.1.4 Load displacement curve

Each sample was loaded until the load-displacement curve begun to assume a downward negative slope after the RHS Ring reached its maximum load carrying capacity.

Fig. 6 (a) shows a typical load-displacement curve from the MTS machine for a RHS Ring (sample SR1) compressed between platens which is used to explain the behavior of RHS Ring compressed between platens. Initially, the curve shows a linear load deflection shape (AB in the graph). This is the elastic region in the graph. At B, the slope of the graph begins to reduce and gradually flattens out at C where the ring reaches its maximum load carrying capacity. Region BC is the elasto-plastic region of the RHS Ring where yielding begins at the outermost fiber on the innermost side and progresses in the thickness direction gradually as the load increases. After reaching a load value at C, the load starts decreasing while the deflection continues to increase (CD in the graph) before the loading was stopped. Region CD is the post-yield region.

Fig. 6 (b) shows the load-displacement curves for the three RHS Rings SR1-SR3 compressed between platens. All three curves display the same trend explained above. Table 2 shows the maximum load values of each of the three samples.

Table 2. Maximum load of RHS rings between platens

RHS ring #	Maximum load (kN)
SR1	0.978
SR2	0.934
SR3	0.900

3.2 Experiment 2– Compression of RHS Rings between Wearpads

3.2.1 Thickness measurement

The thickness measurement taken using a Vernier calipers at points A-J shown in Fig. 3 are listed for the three RHS Ring specimens compressed between wearpads in Table 3.

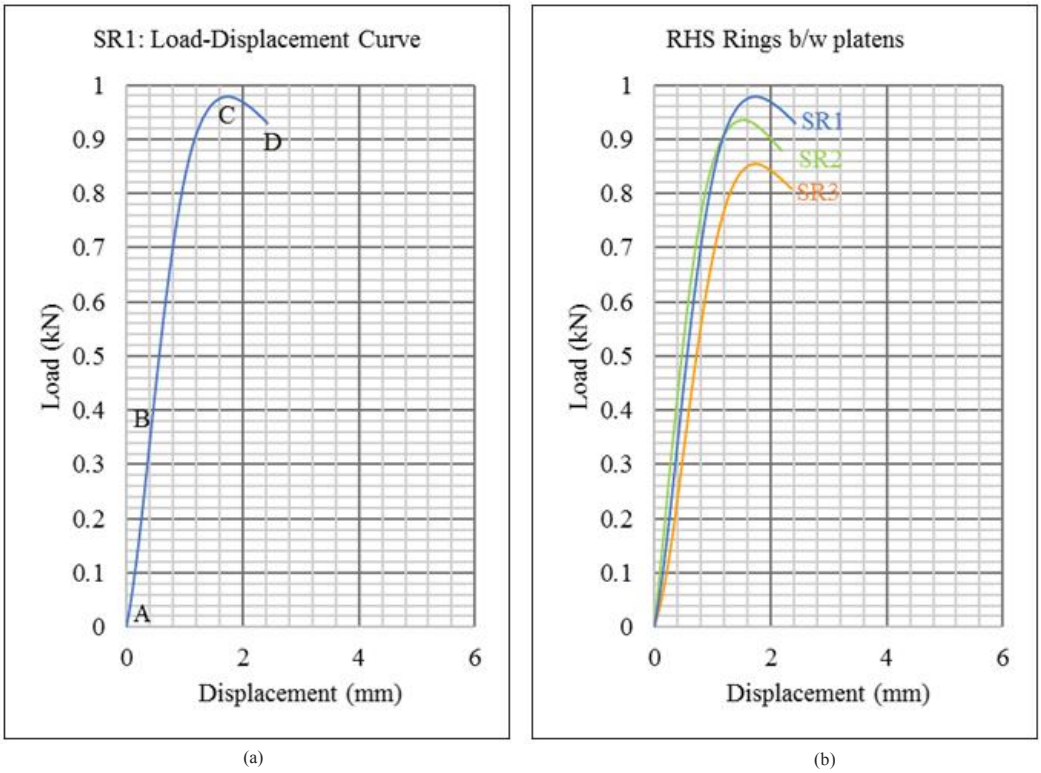

Fig. 6. (a) Typical load-displacement curve (a) Collective Load-displacement curves for RHS Rings between platens

Table 3. Thickness measurements of RHS rings between wearpads

Specimen	Thickness (mm)									
	A	B	C	D	E	F	G	H	I	J
SRW1	3.03	3.08	3.07	3.05	3.03	3.01	3.06	3.07	3.09	3.00
SRW2	3.00	3.10	2.95	2.95	2.94	3.09	3.02	2.97	3.00	3.00
SRW3	3.00	3.06	3.03	3.00	2.99	296	3.05	3.03	3.01	3.02

3.2.2 Description of the process

The assembly of the RHS Ring compressed between wearpads is as shown in Fig. 7 (d). Here again, the top wearpad has a shallow groove on its upper surface to accommodate the load distributor.

The assembly is placed on the lower platen of the MTS machine while the load is applied by the machine top cylinder. The load is continuously applied till the maximum load value is reached after which the load is released and the load-displacement plot is obtained as an output.

3.2.3 Physical behavior

Wearpads are flat cut out surfaces that apply 'patch loads' on portions of the flat, top and bottom flanges of the RHS Rings in contact with them.

Once the load application is started, the top flange starts sagging and the bottom flange starts hogging causing the load distribution to move towards, and eventually concentrate on the outer edges of the wearpads. In short, as the load increases, the wearpads will transmit forces through the areas which maintain contact with the RHS Ring flanges. This is elaborated in Fig. 7 and in the explanation that follows.

Initially, the flanges and the webs showed no deflection and were at right angles to each other as shown in Fig. 7 (a). The flanges maintained area contact only with the regions of the wearpad. As the load is increased, Fig. 7(b) shows the top flange begins to sag (like a beam under transverse loading) and the bottom flange begins to hog causing the flanges to lose contact with the wearpads in the middle. At this stage, the flanges still maintain surface contact with the wearpads. The webs also begin to bulge outwards. A further increase in the load is marked by an obvious and exaggerated deformation on all four strips of the RHS Ring – the two flanges and the two webs as shown in Fig. 7 (c). Contact between the flanges and the wearpads is almost reduced to a line/ edge contact at the outer edges of the wearpads. In the last stage, after the maximum load is passed, the RHS Ring consists of webs hinged at mid-height and bent flanges as shown in Fig. 7(d).

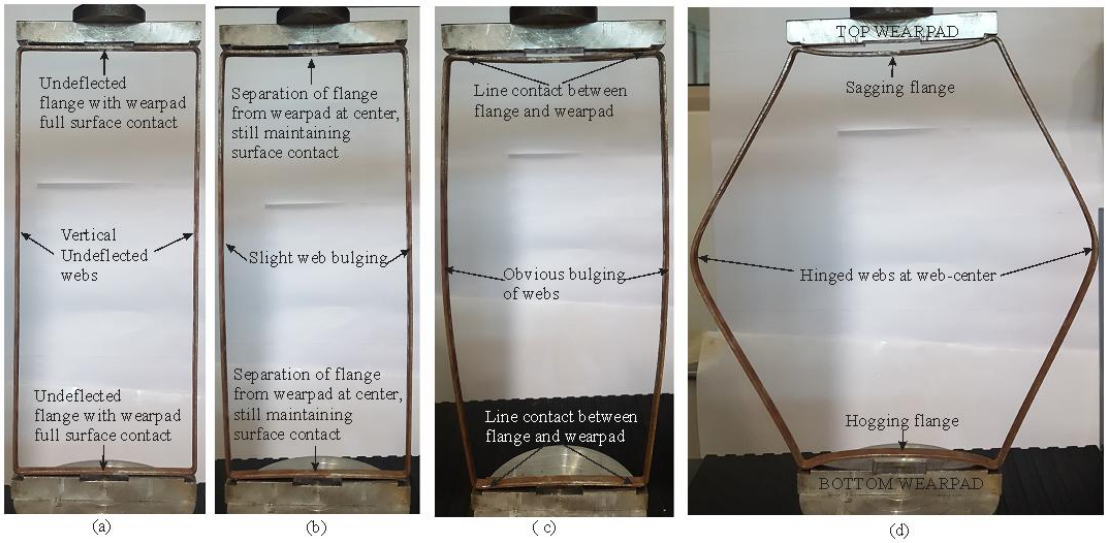

Fig. 7. RHS Ring between wearpads at (a) Stage 1 (b) Stage 2 (c) Stage 3 (d) Stage 4

For compression between wearpads, when the web of the RHS Ring is bent, consider the right web. The bent shape will be as shown in Fig. 8(a). If this is cut by an imaginary plane at the middle, the free body diagram of the upper half will be as shown in Fig. 8(b).

The entire cross section will experience the same compressive stress P/A. In addition, bending stresses are caused by moment due to web deflection 'Py' and moment due to load eccentricity 'Pe' due to the wearpads. This will result in a bigger compressive stress at the outer fiber on the inner side. Yielding therefore can be expected to begin at the inner sides of the flanges at the mid-height at lower load values compared to when loaded between platens.

3.2.4 Load displacement curve

Similar to section 3.1.4, each sample was loaded until the load-displacement curve begun to assume a downward negative slope after the RHS Ring reached its maximum load carrying capacity. Throughout this process the load deflection behavior was recorded.

Fig. 9(a) shows a typical load-displacement curve obtained for a RHS Ring (sample SRW1) compressed between wearpads. Like Fig. 6(a), the load-displacement curve for ring compression between wearpads is marked by points A, B, C, and D as shown in Fig. 9(a). Again, the three main regions are the elastic region (OA), the elasto-plastic region of the reduced slope BC and the post-yield region CD after the maximum load at C.

On comparison with Fig. 6(b), it is observed that the maximum load carrying capacity of RHS Rings between wearpads is smaller than that of RHS Rings compressed between platens. Also, at the maximum load, the displacement in the RHS Ring compressed between wearpads is higher than that observed in RHS Rings compressed between platens. The reasons for both these observations can be attributed to the additional moment caused by the distance of the wearpads from the vertical webs of the RHS Rings.

Fig. 9(b) shows the load-displacement curves for the three RHS Rings SRW1-SRW3 compressed between wearpads. All three curves display the same trend explained above.

Table 4 shows the maximum load values of each of the three samples.

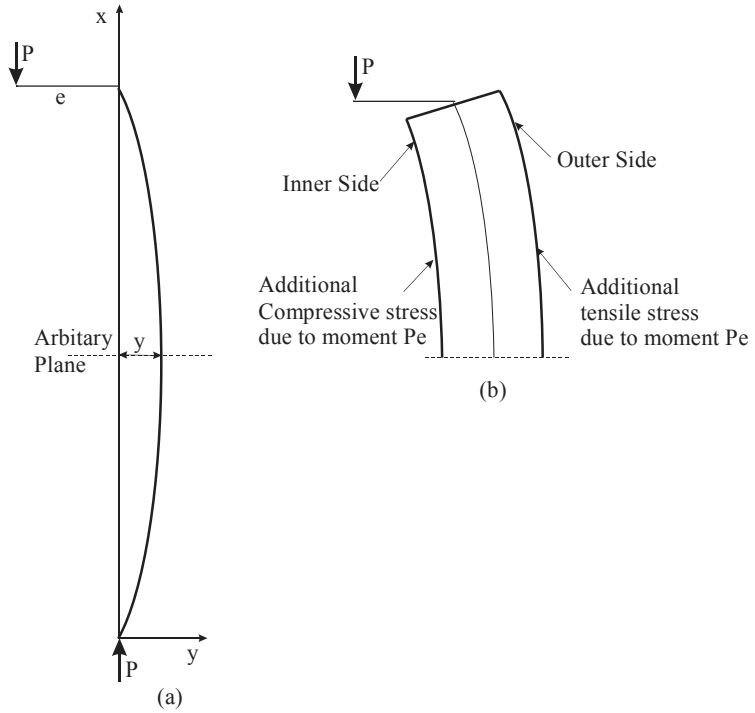

Fig. 8. (a) Eccentric load acting of web (b) Resultant stresses on web

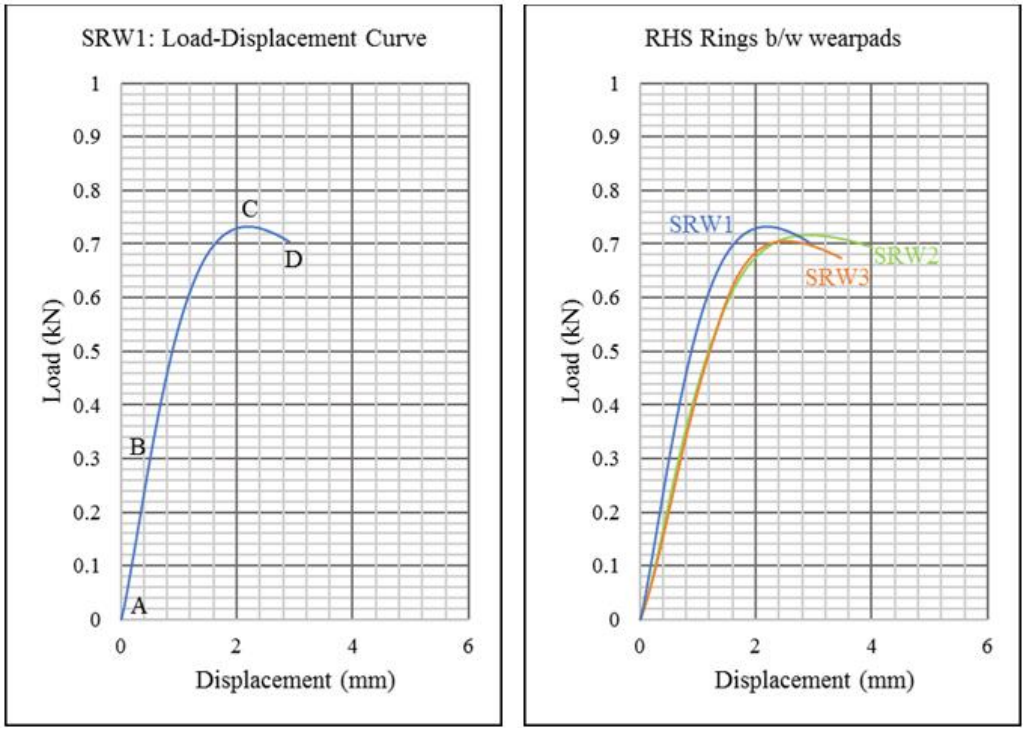

(a) (b)

Fig. 9. (a) Typical load-displacement curve of RHS Ring between wearpads (b) Load Displacement curves of RHS Rings between wearpads

Table 4. Maximum load of RHS rings between wearpads

RHS ring #	Maximum load (kN)
SRW1	0.731
SRW2	0.716
SRW3	0.706

4. FE MODELS

FE models were built for Riks buckling analysis in ABAQUS to represent the physical prototype tested in the experiments shown in section 3. The RHS Rings were built with a height of 350 mm, width of 150 mm, corner radius of 5 mm, length of 10 mm, and a thickness of 3 mm. The platens were built with a 150 mm width with 10 mm length while the rectangular extrusions were assigned a width of 55 mm, length of 10 mm, with a distance of 10 mm from the edge. The FE model assemblies are shown in Fig. 10.

The material properties from a test coupon of the sheet used to fabricate the RHS Rings were assigned to all parts in both assemblies. The material properties were: Modulus of Elasticity = 125,946 N/mm^2, Yield Stress = 211.88 N/mm^2, Ultimate Stress = 317.35 N/mm^2, and density = 7.89E-09 tonne/mm^3.

4.1 RHS Ring between Platens

Details of modelling and analysis are described below.

4.1.1 Assembly and interactions

A typical FE model comprising of three parts—the top platen, the bottom platen, and the RHS Ring is shown in Fig. 10 (a).

The bottom outer face of the RHS Ring is assigned a frictional interaction with the bottom platen. The bottom platen is encastred, thereby restricting all degrees of freedom. The top outer face of the RHS Ring is assigned a frictional interaction with the underside of the top platen and the all degrees of freedom of the top platen were restrained apart from the vertical translation, thereby allowing for compression. A reference point RP-1 was created at the center of the top face of the top platen and kinematically

coupled with the top platen top surface for uniform application of the load on the top platen.

4.1.2 Finite element mesh and element

The platens were assigned a solid element C3D8R and the RHS Ring a shell element S4R. The S4R element is a general purpose element, with reduced integration [14]. Due to the reduced integration, the locking phenomenon observed in the S4 element does not show.

A mesh analysis resulted in determining a size of 5 mm ×5 mm for both parts.

4.1.3 Results

The analysis was a one-step Riks analysis where a displacement of -15 was applied through RP-1 in the Riks step. The comparison of the load-displacement curves between the three experimental samples and the FE Model is shown in Fig. 11. The red curve indicates the load-displacement curve for the FE Model, while the three blue curves are the load-displacement curves experimentally obtained in section 3.1.4. Fig. 11 indicates that the load-displacement curve from the FEA is in agreement with that obtained from the experiments.

From the FE model, a maximum load of 0.905 kN was acquired. This was in agreement with the maximum load values acquired from the three samples tested experimentally shown in Table 2.

4.2 RHS Ring between Wearpads

Details of modelling and analysis are described below.

4.2.1 Assembly and interactions

The platens in section 4.1.1 are replaced by the top and bottom wearpads in this section. The wearpads are built by extruding two rectangular cubes from the wearpad platens as shown in Fig. 10(c). A typical FE model representing RHS Ring compression between wearpads is as shown in Fig. 10(b).

The bottom face of the RHS Ring is assigned a frictional interaction with the two extrusions of the bottom wearpad. The bottom wearpad platen is encastred, thereby restricting all degrees of freedom. The top outer face of the RHS Ring is assigned a frictional interaction with the two extrusions of the top wearpad and all degrees of freedom of the top wearpad platen were restrained apart from the vertical translation, thereby allowing for compression. Similar to section 4.1.1, a reference point RP-1 was created at the center of the top face of the top wearpad platen. RP-1 was kinematically coupled with the top wearpad platen top surface for uniform application of the load on the top wearpad.

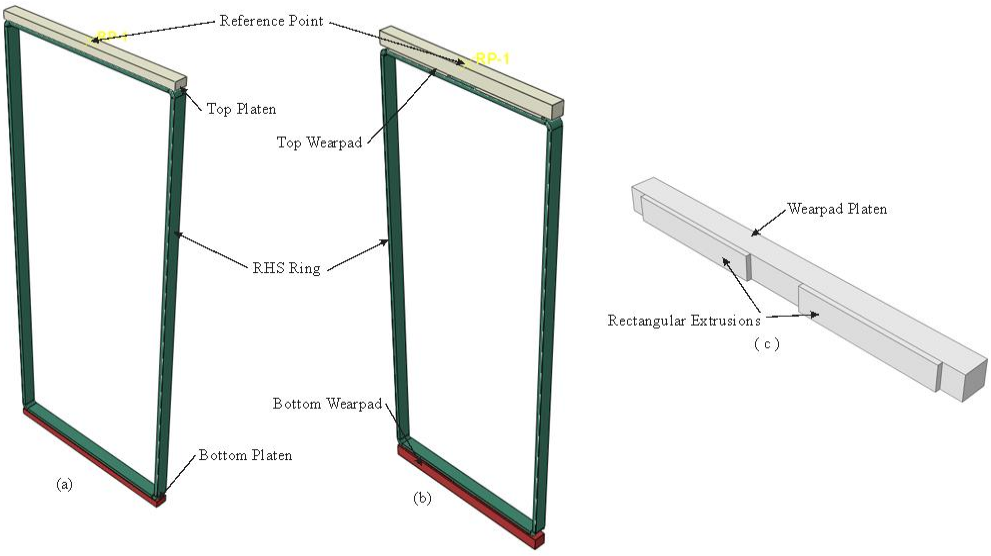

Fig. 10. (a) RHS Ring between platens (b) RHS Ring between wearpads (c) Wearpad assembly

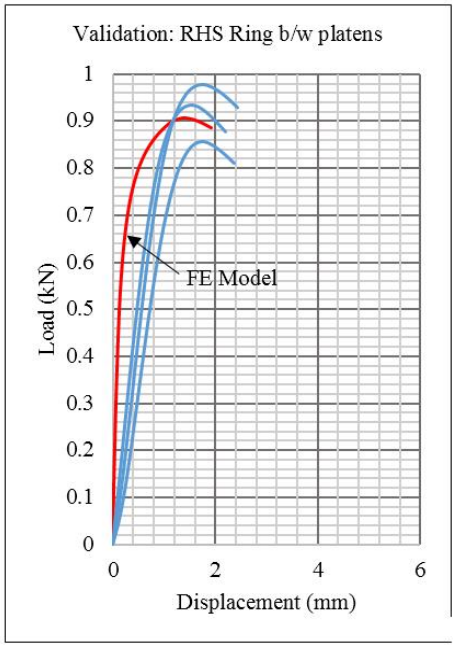

Fig. 11. Load-Displacement curve validation for RHS Rings between platens

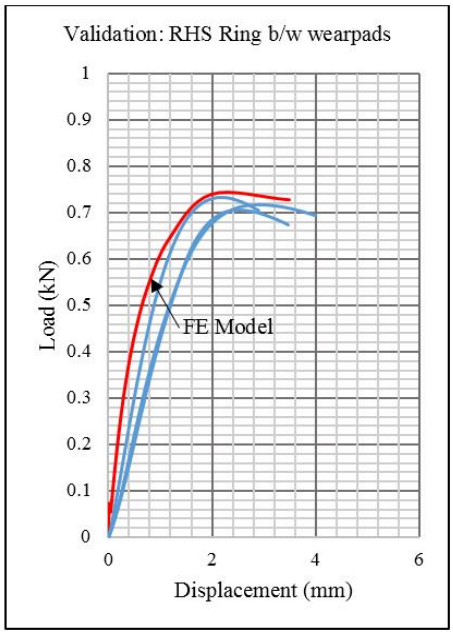

Fig. 12. Load-Displacement curve validation for RHS Ring between wearpads

4.2.2 Finite element mesh and element

The wearpads were assigned a solid element C3D8R and the RHS Ring a shell element S4R. A mesh analysis resulted in determining a size of 5 mm ×5 mm for both parts.

4.2.3 Results

The load-displacement comparison plot between the three experimental samples and the FE Model is shown in Fig. 12. The red curve indicates the load-displacement curve for the FE Model, while the three blue curves are the load-displacement curves experimentally obtained in section 3.2.4. The load-displacement curves obtained from the two methods are found to be in agreement.

For RHS Ring compression between wearpads, a maximum load of 0.738 kN was acquired from the FE model. This was in agreement with the maximum load values acquired from the three samples tested experimentally shown in Table 4.

5. THEORETICAL EXPLANATION

5.1 RHS Ring between Platens

A rectangular ring is made up of two flanges and two webs as shown in Fig. 13(a). The load is applied by the platens on the flanges. At the beginning, this can be considered as a uniformly distributed load. This load has to be taken up by the webs. This means that the top flange will have two upward reactions from the webs. If a beam is supported at the ends and a distributed or pressure load is applied, the result will be a bent beam as shown in Fig. 13(b). This bending will increase as the load applied increases. The platen is a flat surface and because of the bending the middle of the platen will lose contact with the middle of the beam as shown in Fig. 13(c). In the limiting condition, the platen will have contacts at the extreme points only, i.e. near the webs, and there will only be a line contact (represented by a point in the 2D representation as shown in Fig. 13(d). It is therefore safe to assume that the webs directly take up the load and the flanges are free from the load. This explanation is in agreement with the behavior of the rings compressed between platens in the experiments in section 3.1.3.

Further, the sagging of the top flange will try to rotate the flange at the ends. But the webs will resist this rotation and create reaction moments at the joints. In the limiting condition, the loading in the flange can be assumed to be as shown in Fig. 14(a). Considering the webs, the reaction moments in the flanges have to be balanced for equilibrium, in the corners where the flanges meet the webs. To meet this requirement the webs will have reaction moments acting in the

opposite directions to those in the flange. The loadings in the right web are shown in Fig. 14(b).

In summary when a rectangular ring is loaded between platens, the flanges will behave like beams subjected to end moments and forces. The webs will behave like columns subjected to compressive loads and end moments. This is similar to a column with eccentric loading. Fig. 15 schematically represents the ring under loading between platens.

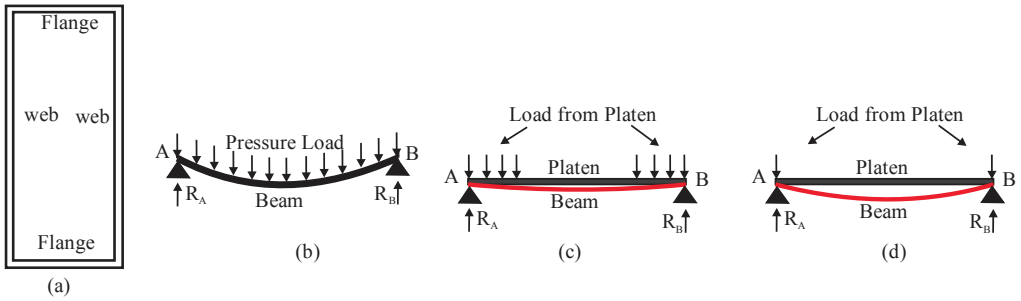

Fig. 13. Rectangular section and loading at the top flange by the platen

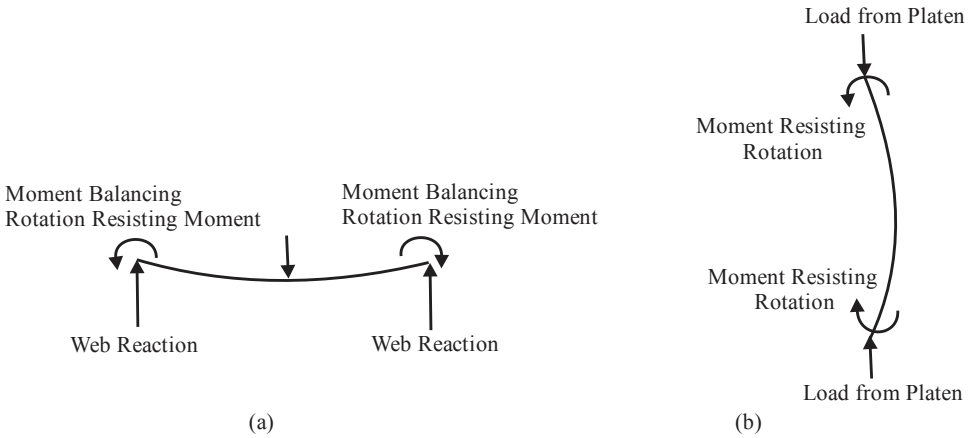

Fig. 14. Loadings in the flanges and webs of a ring

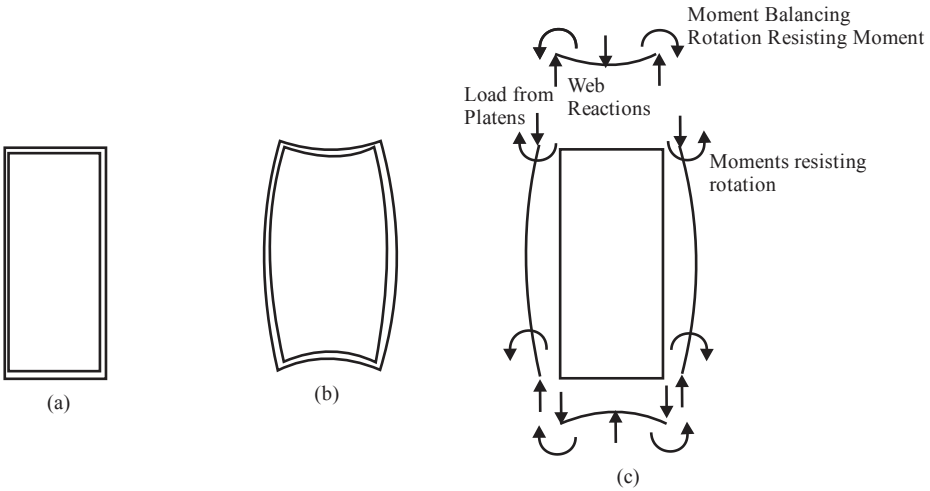

Fig. 15. (a) Unloaded RHS Ring (b) Deformed RHS Ring Shape(c) Force Diagram of RHS Ring under Loading between Platens

5.1.1 Analysis of the web of a rectangular ring

Now consider the left web in the slightly bent position as shown in Fig. 16. This web takes half of the load from the platens at both ends. Fig. 16(a) represents the left web.

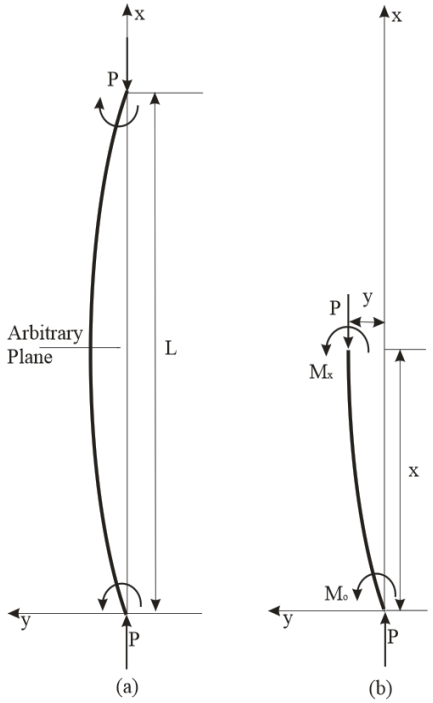

Fig. 16. (a) Deformed left web (b) forces and moments on section of left web

The free body diagram shown in Fig. 16(b) shows the bending moment in a section at a distance x from the y axis along the x axis. The bending moment is

The bending moment is

$$M_x = -M_0 - Py \tag{1.1}$$

The governing differential equation is

$$EI\frac{d^2y}{dx^2} + Py = -M_0 \tag{1.2}$$

Substituting $k^2 = \frac{P}{EI}$ in (4.2), the differential equation is

$$\frac{d^2y}{dx^2} + k^2y = -\frac{M_0}{EI} \tag{1.3}$$

Its boundary conditions are $y = 0$ when $x = 0$ and $x = L$

The general solution for this differential equation is

$$y = A\cos kx + B\sin kx \tag{1.4}$$

Its particular solution can be of the form $y_p = C$ and the complete solution is

$$y = A\cos kx + B\sin kx + C$$

Substituting for y_p and its derivatives in (4.3) gives

$$k^2(C) = -\frac{M_0}{EI}$$

$$\therefore C = -\frac{M_0}{EI \times k^2} = -\frac{M_0}{P} \quad \left(\because k = \sqrt{\frac{P}{EI}}\right)$$

The full solution is

$$y = A\cos kx + B\sin kx - \frac{M_0}{P} \tag{1.5}$$

Substituting the boundary conditions gives

$$A = \frac{M_0}{P} \text{ and } B = \frac{M_0}{P}\left(\frac{1-\cos kL}{\sin kL}\right) = \frac{M_0}{P}\tan\left(\frac{kL}{2}\right)$$

The full solution is

$$y = \frac{M_0}{P}\left(\cos kx + \tan\left(\frac{kL}{2}\right)\sin kx - 1\right) \tag{1.6}$$

Differentiating once gives

$$y' = \frac{M_0}{P}\left(-k\sin kx + k\tan\left(\frac{kL}{2}\right)\cos kx\right) \tag{1.7}$$

When $x = 0$, $y' = \frac{M_0}{P}\left(k\tan\left(\frac{kL}{2}\right)\right)$

5.1.2 Analysis of the bottom flange of a rectangular ring

Consider a beam with both ends simply supported.

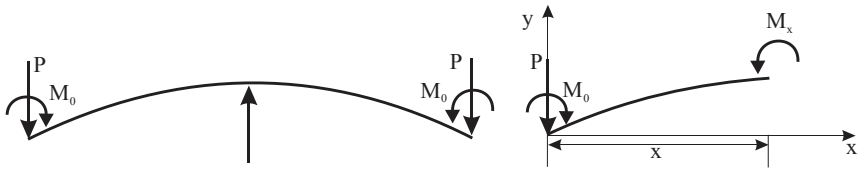

Fig. 17. Forces and moments in the bottom flange

The bending moment is

$$M_x = M_0 - Px \tag{1.8}$$

The governing differential equation is

$$EI\frac{d^2y}{dx^2} = M_0 - Px \tag{1.9}$$

Integrating once gives

$$EI\frac{dy}{dx} = M_0 x - \frac{Px^2}{2} + C \tag{1.10}$$

Integrating again gives

$$y = \frac{1}{EI}\left[\frac{M_0 x^2}{2} - \frac{Px^3}{6} + Cx + D\right] \tag{1.11}$$

Substituting $x = \frac{l_1}{2}$, $\frac{dy}{dx} = 0$ and $x = 0$, $y = 0$ in (1.10) and (1.11) gives

$$D = 0;\ C = \frac{1}{8}\left[Pl_1^2 - 4M_0 l_1\right] \tag{1.12}$$

Substituting (1.12) in (1.11) gives

$$y = \frac{1}{EI}\left[\frac{M_0 x^2}{2} - \frac{Px^3}{6} + \frac{1}{8}\left[Pl_1^2 - 4M_0 l_1\right]x\right] \tag{1.13}$$

Deflections at mid-point,

$$\therefore \delta_1 = \frac{1}{8EI}\left[-M_0 l_1^2 + \frac{1}{3}Pl_1^3\right] \tag{1.14}$$

5.2 RHS Ring between Wearpads

The load in this setup is applied by the wearpads on the flanges. At the beginning, this can be considered as uniformly distributed loads on two sections of a beam as shown in Fig.18(a). As the load increases the bending will also increase and separation between the wearpads and the flange will begin as shown in Fig. 18(b).

The bending will increase further as the load applied increases and in the limiting condition the wearpads will have contacts at the extreme points only, i.e. near the webs, and there will only be a line contact. The forces will be similar to those shown in Fig.18(c). This explanation is in agreement with the behavior of the RHS Rings compressed between wearpads in the experiments in section 3.2.3.

Now consider the force system in Fig. 19(a) where two forces P act at A and B at a distance *a* from the flange ends C and D. If two forces of the same magnitude as P, and opposite in direction act at each of the flange ends at C and D as shown in Fig. 19(b), they would not make any difference to the system. Now, the force at A and the force opposite in direction at point C form a couple. Similarly, the force at B and the force opposite in direction at point D form a couple. Therefore, the forces acting at A and B in Fig. 19(a) can be represented by forces and moments acting at C and D in the direction shown in Fig. 19(c). The two vertical forces at C and D shown in Fig. 19(c) can be replaced by a single vertical force 2P acting at the flange center shown in Fig. 19(d). This force 2P is balanced by the reaction forces at C and D shown in Fig. 19(d). The moments caused by the wearpads shown in Fig. 19(c) cause counter reaction moments of the same magnitude from the flange as shown in Fig. 19 (d).

Thus mathematically, loading through the wearpads is equivalent to creating an additional moment to the system compared to when loading is through the platens. These additional moments cause reaction moments that act in the same directions as the moments created when loading is through platens. Since the webs and flanges are connected, these reaction moments also have to come from the web and will be in the opposite direction to the reaction moments at the flanges. Fig. 20 schematically represents the loading under wearpads.

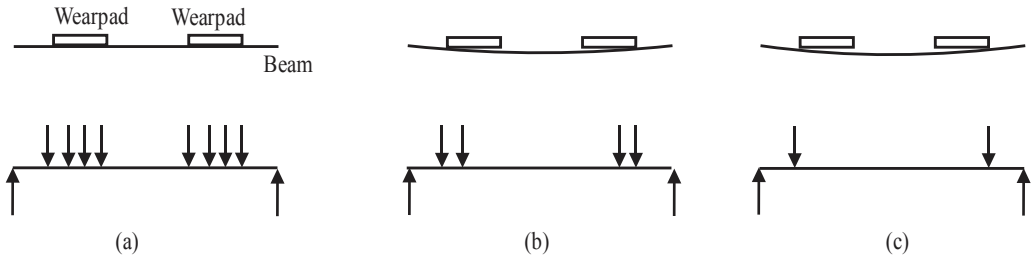

Fig. 18. Loading through Wearpads

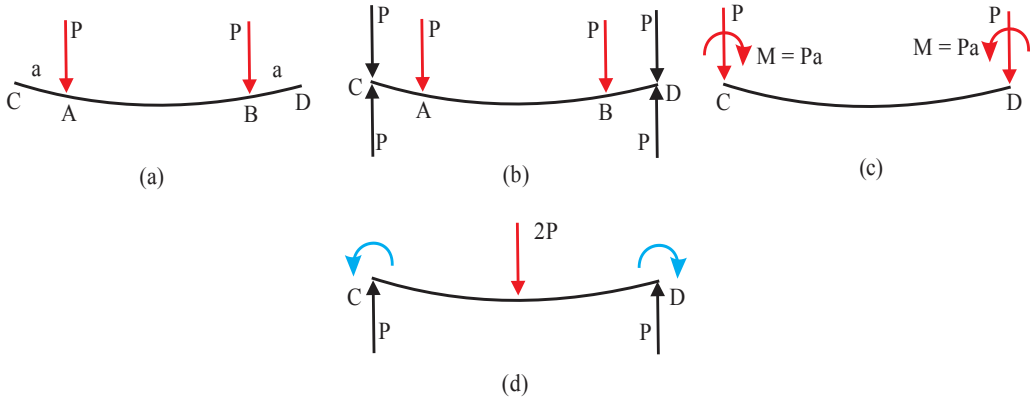

Fig. 19. Load at the right half of the flange

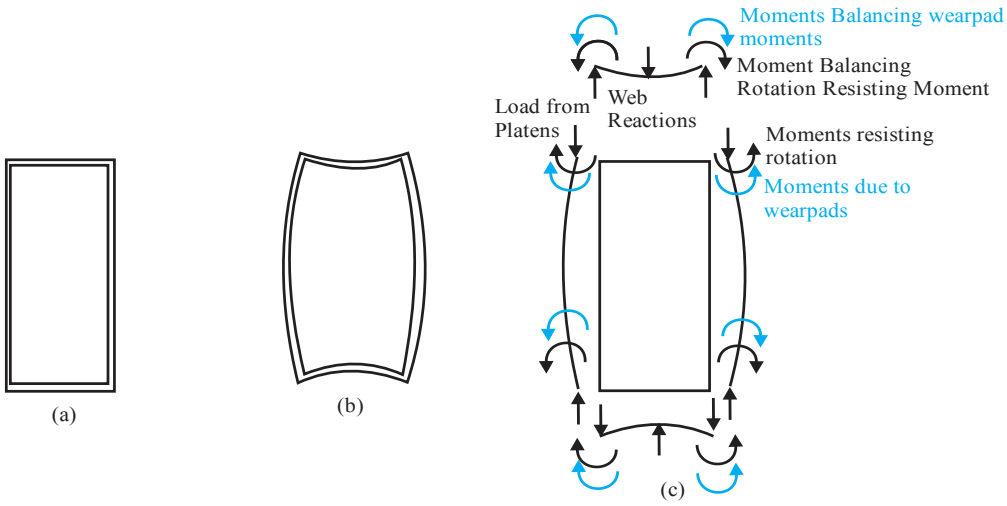

Fig. 20. Unloaded RHS Ring (b) Deformed RHS Ring Shape (c) Force Diagram of RHS Ring under Loading between wearpads

6. CONCLUSIONS

a. Experimental transverse compression of RHS Rings under transverse compressive loads between both platens and wearpads show concave inward bending of the flanges and outward bulging of the webs. As the applied load increases, the flanges of the RHS Ring separate from the platens or the wearpads and in the limiting condition, contact between the RHS Ring flanges and the platens or wearpads reduces to a line contact.

Also, for a given set of geometrical factors, the maximum load value of a RHS Ring compressed between wearpads is lower than the maximum load of a RHS Ring compressed between platens. Experimentally, the load deflection curves are characterized by three distinct areas; the elastic region, the elasto-plastic region and a post-ultimate region.

b. The FE models of RHS Rings between platens and wearpads show load-displacement graphs, maximum load values and deformed shapes in agreement with that obtained from the experiments.

c. The behavior of the RHS Rings compressed under transverse loads can be explained theoretically by analyzing the ring as an assemblage of two columns (webs) and two beams (flanges). The applied compressive loads cause each member of the ring to be subjected to end moments and end reaction forces. The webs in a ring can therefore be considered as a column under eccentric loading (because of the end reaction moments). The boundary conditions for the web under axial compression is neither pinned nor fixed. This means that the value for k_1 in the equation $P_{cr} = \frac{k_1 \pi^2 EI}{L^2}$ is between 1 and 4. Stresses at the mid-height of the web are due to (a) the axial compression and (b) bending as a beam. Axial compressive stress is uniform throughout the cross section. The bending stress is compressive maximum at the inner fiber and tensile maximum at the outer fiber. This means that yielding will start at the inner fiber and progress outwards. The end moments on the flanges cause bending stresses which can cause yielding at the mid span. Loading through wearpads causes additional end moments to act on all the members of the RHS Ring. These additional end moments reduce the magnitude of load P at which the RHS Ring starts yielding. These additional end moments also cause higher lateral displacements at the web center when compared to platen loading. The effect of the additional corner moments because of wearpad loading was also observed in the experiments.

COMPETING INTERESTS

Authors have declared that no competing interests exist.

REFERENCES

1. Reddy TY, Reid SR. Phenomena associated with the crushing of metal tubes between rigid plates. Int. J. Solids Struct. 1980;16(6):545–562.
2. Sinha DK, Chitkara NR. Plastic collapse of square rings. Int. J. Solids Struct. 1982;18(9):819–826.
3. Gupta NK, Khullar A. Collapse load analysis of square and rectangular tubes subjected to transverse in-plane loading. Thin-Walled Struct. 1995;21(4):345–358.
4. Gupta NK, Khullar A. Lateral collapse of orthogonal and non-orthogonal cross-layered arrays of square and rectangular tubes. Int. J. Mech. Sci. 1994;36(5):449–467.
5. Gupta NK, Ray P. Collapse of thin-walled empty and filled square tubes under lateral loading between rigid plates. Int. J. Crashworthiness. 1998;3(3):265–285.
6. Gupta NK, Sinha SK. Transverse collapse of thin-walled square tubes in opposed loadings. Thin-Walled Struct. 1990;10(3): 247–262.
7. Gupta NK, Sinha SK. Collapse of a laterally compressed square tube resting on a flat base. Int. J. Solids Struct. 1990;26(5):601–615.
8. Gupta NK, Khullar A. Lateral crushing of square and rectangular tubes by non-orthogonally placed narrow width indenters. Int. J. Mech. Sci. 1995;37(1): 31–50.
9. Gupta NK, Khullar A. Lateral compression of a square or rectangular tube between two parallel narrow width indenters placed non-orthogonally. Thin-Walled Struct. 1995;22(1):9–23.
10. Gupta NK, Sekhon GS, Gupta PK. A study of lateral collapse of square and rectangular metallic tubes. Thin-Walled Struct. 2001;39(9):745–772.
11. Fan H, Hong W, Sun F, Xu Y, Jin F. Lateral compression behaviors of thin-walled equilateral triangular tubes. Int. J. Steel Struct. 2015;15(4):785–795.

12. Leu DK. Finite-element simulation of the lateral compression of aluminium tube between rigid plates. Int. J. Mech. Sci. 1999;41(6):621–638.
13. Tran TN, Ton TNT. Lateral crushing behaviour and theoretical prediction of thin-walled rectangular and square tubes. Compos. Struct. 2016;154:374–384.
14. Abaqus Analysis User's Manual (6.12). [Online]. Available:http://abaqus.software.polimi.it/v6.12/books/usb/default.htm?startat=pt06ch28s01ael03.html [Accessed: 22-Dec-2016]

Peer-review history:
The peer review history for this paper can be accessed here:
http://sciencedomain.org/review-history/22013